Green Chemistry

PAPER

View Article Online
View Journal

Cite this: DOI: 10.1039/d6gc00241b

A multi-enzyme cascade with internal cofactor cycling for the green conversion of inert *n*-alkanes to α,ω-dicarboxylic acids

Zhijun Kong,[a] Weihan Sun,[a] Wenjin Dong,[a] Su Song,[a] Li Ma,*[a] Shengying Li *[a,b] and Hui Chen *[a]

The selective conversion of chemically inert linear alkanes into α,ω-dicarboxylic acids remains a significant challenge in sustainable chemistry. α,ω-Dicarboxylic acids are key building blocks for high-performance polymers and pharmaceuticals, their industrial production relies on energy-intensive, poorly selective multi-step oxidation processes. These limitations stem from the intrinsic inertness of inactivated primary C–H bonds and the difficulty of achieving regioselective dual-terminal C–H bond oxyfunctionalization under mild conditions. Consequently, progress in the conversion of chemically inert linear alkanes into α,ω-dicarboxylic acids hinges on two central challenges: enabling highly regioselective terminal C–H oxidation and developing sustainable transformation pathways. To address these challenges, we developed a multi-enzyme cascade driven by internal cofactor cycling that enables one-pot deep oxidation of dodecane to dodecanedioic acid under mild conditions. In the first stage, a hydrogen-borrowing-based NADH regeneration strategy enables selective oxidative C–H functionalization, converting dodecane to dodecanoic acid. Coupling this step with a second hydrogen-borrowing cycle and *in situ* elimination of H_2O_2 further drives terminal oxidation, ultimately affording 1.49 mM dodecanedioic acid. In addition, nonane, decane, undecane, and tridecane were successfully converted into their corresponding α,ω-dicarboxylic acids. Overall, this study establishes a green biocatalytic paradigm for the deep transformation of inert alkanes using molecular oxygen as the sole oxidant, enabled by internal cofactor cycling and *in situ* reactive oxygen management. This strategy maximizes atom economy and provides an efficient and sustainable route for upgrading linear alkanes into value-added products.

Received 24th January 2026,
Accepted 27th April 2026

DOI: 10.1039/d6gc00241b

rsc.li/greenchem

Green foundation

1. This work advances green chemistry by enabling efficient, waste-minimized conversion of inert fossil-based alkanes into valuable α,ω-dicarboxylic acids through a high-performance biocatalytic platform that embodies atom economy and energy-efficient processing.
2. We developed a self-sustaining multi-enzyme redox cascade that converts inert C_9–C_{13} alkanes into α,ω-dicarboxylic acids with >99% terminal selectivity. The system relies entirely on internal NADH recycling, producing various α,ω-dicarboxylic acids without sacrificial co-substrates, maximizing atom economy and process efficiency.
3. Future work will enhance enzyme efficiency, stability, and reuse through protein engineering and immobilization to improve atom economy and space–time yield. Transitioning from petrochemical alkanes to renewable, bio-derived feedstocks will further strengthen the sustainability and circularity of this biocatalytic platform.

Introduction

Dicarboxylic acids (DCAs), a class of linear α,ω-dicarboxylic acids, are essential monomers for the manufacture of high-performance engineering plastics, specialty polymers, plasticizers, fragrances, and pharmaceutical intermediates.[1,2] The global market for long-chain DCAs continues to expand, driven by the increasing demand for sustainable materials with excellent thermal and mechanical properties.[3,4] However, conventional industrial routes for DCA production rely heavily on multi-step chemical processes that are both energy-intensive and environmentally detrimental. For instance, in the industrial manufacture of adipic acid, cyclohexane is first partially oxidized to a cyclohexanol/cyclohexanone mixture

[a]State Key Laboratory of Microbial Technology, Shandong University, Qingdao 266237, China. E-mail: maliqd@sdu.edu.cn, lishengying@sdu.edu.cn, Chen.Hui@sdu.edu.cn
[b]Laboratory for Marine Biology and Biotechnology, Qingdao Marine Science and Technology Center, Qingdao 266237, China

(commonly referred to as KA oil), which is subsequently oxidized with concentrated nitric acid in a separate step.[5–7] This nitric-acid oxidation requires elevated temperatures (70–170 °C) and excess oxidant, resulting in high energy consumption and low process efficiency. Moreover, this step inevitably generates large quantities of nitrous oxide (N_2O), a potent greenhouse gas with a global warming potential approximately 300 times greater than that of carbon dioxide.[5–8] In addition to N_2O emissions, the nonselective nature of nitric-acid oxidation leads to the formation of structurally similar byproducts, such as succinic and glutaric acids. Their separation from the target product requires energy-intensive, multi-stage crystallization and purification processes, significantly reducing atom economy and increasing waste generation.[8,9] Consequently, this high-carbon-emission, low-selectivity, and resource-inefficient production route stands in sharp contrast to the principles of green chemistry and the urgent goals of carbon neutrality.

Breakthroughs in synthetic biology have opened new avenues for the green manufacturing of DCAs. Current strategies for DCA biosynthesis predominantly focus on constructing efficient microbial cell factories through metabolic engineering and strain improvement. These approaches generally comprise three core dimensions. At the level of substrate uptake, transmembrane mass-transfer limitations associated with hydrophobic substrates are addressed by introducing or overexpressing specific transporters, such as AlkL or CtFat1p.[10–12] At the catalytic conversion level, the native ω-oxidation pathway is reinforced by integrating highly regioselective monooxygenases with dehydrogenase systems to enhance terminal oxidation efficiency.[8,13,14] At the level of metabolic flux regulation, gene-editing strategies are employed to block competing β-oxidation pathways, thereby directing carbon flux preferentially toward DCA biosynthesis.[15–18] Although microbial fermentation utilizing glucose, fatty acids, or even *n*-alkanes has achieved high product titers, whole-cell biocatalysis is inherently constrained by the competition for carbon sources between cell growth and product synthesis, resulting in limited atom economy. Straight-chain alkanes, have garnered significant attention fundamental feedstocks in the petrochemical industry, owing to simple molecular structures and abundant reserves; however exhibit highly inert C–H bonds and low chemical reactivity.[19–21] Compared with fatty acids and oil-based substrates, which have been extensively explored, the biocatalytic upgrading of straight-chain alkanes remains far less developed. The development of a biocatalytic system capable of directly converting straight-chain alkanes into DCAs would not only significantly streamline synthetic routes but also fundamentally circumvent the environmental burdens associated with conventional chemical processes. However, two fundamental challenges still hinder progress in this field: (i) achieving sustainable and highly regioselective dual-terminal C–H functionalization of linear alkanes under mild conditions, and (ii) designing flexible and sustainable catalytic pathways capable of efficiently orchestrating these complex multi-step transformations. Therefore, developing sustainable strategies for constructing such frameworks is of great significance. Highlighting this significance, the ACS Green Chemistry Institute® Pharmaceutical Roundtable (GCIPR) identified "aliphatic and aromatic C–H activation, using green oxidants and giving predictable site selectivities" as a key research area in 2018, underscoring the demand for efficient, environmentally benign alternatives.[22]

The ubiquitous C–H bond is intrinsically inert owing to high bond dissociation energy.[23,24] Conventional activation strategies typically rely on precious transition-metal catalysts (*e.g.*, Pd, Rh) or aggressive radical initiators under harsh conditions.[8,25] However, these approaches generally exhibit poor regioselectivity, particularly along aliphatic chains, and depend on hazardous oxidants, causing low atom economy and toxic byproducts.[26,27] In contrast, enzymatic C–H bond functionalization offers inherent advantages in regioselectivity, stereoselectivity, and substrate specificity.[28] These biocatalytic transformations proceed under mild aqueous conditions and often exhibit high catalytic efficiency.[29] Nevertheless, enzymes capable of dual-terminal C–H functionalization are rare in nature, as most metabolic pathways require modification at only a single terminal position. Consequently, research on enzymatic terminal C–H bond oxyfunctionalization has primarily focused on two major enzyme classes: alkane hydroxylase (AlkB) and cytochrome P450 fatty acid hydroxylases belonging to the CYP153 family. AlkB systems, such as those derived from *Pseudomonas putida* GPo1, catalyze the regioselective activation of single-terminal C–H bonds in C_5–C_{12} alkanes through a three-component electron transfer chain consisting of AlkB, rubredoxin (AlkG), and rubredoxin reductase (AlkT).[30–33] The CYP153A family represents a distinct group of class I cytochrome P450 monooxygenases that require ferredoxin (Fdx) and ferredoxin reductase (FdR) for electron transfer and are specialized in terminal ω-hydroxylation of alkanes and fatty acids. Among them, $CYP153A_{Maq}$ from *Marinobacter aquaeolei* has been extensively investigated.[34,35] This enzyme exhibits excellent regioselectivity (>95%) toward ω-hydroxylation of fatty acids with chain lengths ranging from C_9 to C_{20}.[36]

Building upon the efficient oxyfunctionalization of C–H bonds, the rational design and integration of downstream multi-step reaction processes are essential for the deep conversion of chemically inert alkane into value-added products. In this context, *in vitro* multi-enzyme cascade catalysis offers an attractive solution. By modularly assembling enzymes from different biological origins, continuous catalytic pathways can be constructed in a single reactor without reliance on protecting groups, thereby avoiding intermediate isolation, minimizing chemical waste, and eliminating protection–deprotection steps.[30,37,38] More importantly, the flexibility of *in vitro* cascade systems enables the design of artificial and shortened reaction routes that bypass the complexity of cellular metabolism. Such streamlined pathways reduce the number of reaction steps, maximize theoretical yields, and substantially improve the overall atom economy of the process.[39] However, these cascade reactions are typically dependent on nicotinamide cofactors

(NAD(P)H/NAD(P)$^+$), and their stoichiometric consumption significantly increases operational costs.[40] Conventional cofactor regeneration strategies, such as formate dehydrogenase/formate systems, partially mitigate this issue but require sacrificial substrates and often introduce undesired side reactions, thereby compromising atom economy and process sustainability.[41–43] In recent years, biocatalytic hydrogen borrowing has emerged as a powerful alternative, owing to its exceptional atomic efficiency and thermodynamically self-sustaining nature.[44] In this mechanism, two enzyme-catalyzed half-reactions are intrinsically coupled: during the oxidative half-cycle, hydride equivalents released from substrate dehydrogenation are captured by NAD^+ to form NADH; during the reductive half-cycle, NADH subsequently transfers the hydride to another substrate, regenerating NAD^+.[45] This closed-loop hydrogen-borrowing design eliminates the need for external sacrificial reagents and enables unidirectional cascade progression driven by a favorable free energy gradient.[30] By establishing an internal hydrogen economy, this strategy not only enhances process efficiency and sustainability but also simplifies reaction engineering by preventing the accumulation of regeneration byproducts that may inhibit enzyme activity or complicate downstream purification.

In this study, we address a key challenge in green alkane valorization by developing a tailored *in vitro* multi-enzyme cascade for the deep conversion of linear alkanes. The cascade integrates an alkane hydroxylase (AlkB, EC 1.14.15.3) from *Pseudomonas putida* GPo1,[30–32] an engineered choline oxidase ($AcCO_6$, EC 1.1.3.17) from *Arthrobacter chlorophenolicus*,[46,47] an aldehyde dehydrogenase (EcALDH, EC 1.2.1.5) from *Escherichia coli* K-12,[48] and an engineered cytochrome P450 ω-hydroxylase ($CYP153A_{Maq}$, EC 1.14.15.3) from *Marinobacter aquaeolei*.[35] We demonstrate efficient, highly regioselective dual-terminal C–H bond activation system under mild conditions, using molecular oxygen as the sole oxidant and water as the green solvent. Central to this strategy is the implementation of an internal hydrogen-borrowing mechanism, which enables autonomous NAD(H) recycling without external sacrificial substrates. This work establishes a concise, atom-economical, and sustainable biocatalytic paradigm for upgrading chemically inert alkanes, providing a green alternative to conventional energy-intensive and high-emission synthetic routes.

Materials and methods

Chemicals, bacterial strains, and medium

Unless stated otherwise, all chemicals were purchased from Aladdin (Shanghai, China). The strains *E. coli* C43(DE3)-pET-20b-*alkb*, *E. coli* BL21(DE3)-pET-20b-*alkg*, *E. coli* BL21(DE3)-pET-20b-*acco*$_6$, *E. coli* BL21(DE3)-pET-20b-*aldh*, BL21(DE3)-pET-20b-*cata*, and BL21(DE3)-pET-28a-*pdr* were all obtained from our laboratory collection. The recombinant plasmid pET-20b-$CYP153A_{Maq}$ was synthesized and constructed by Genscript, Inc. Luria–Bertani (LB) medium was used for *E. coli* cell culture and recombinant protein expression, Terrific Broth (TB) medium was used for $CYP153A_{Maq}$ and Pdx expression. The final concentration of antibiotics used for the culture of *E. coli* cell harbored foreign plasmid and the expression of recombinant proteins was 100 mg L^{-1} ampicillin (*E. coli* harbored plasmids with pET-20b backbone) or 50 mg L^{-1} kanamycin (*E. coli* harbored plasmids with pET-28a backbone).

Expression and purification of enzymes with His-tag

E. coli BL21(DE3) strain containing expression plasmids of EcALDH, $AcCO_6$, PdR and CatA proteins was inoculated into LB medium and cultured at 37 °C until the OD_{600} reached 0.6–0.8. IPTG was then added to a final concentration of 0.5 mM, and the culture temperature was adjusted to 16 °C for induced expression for 16–20 hours. Cells were harvested by centrifugation at 6000*g* for 10 minutes. The cell pellet was resuspended in 50 mM KPi buffer (pH = 7.2), sonicated, and then centrifuged at 12 000 rpm for 1.5 hours. Load the supernatant onto a HisPrep™ FF 16/10 chromatography column (Cytiva, Amersham, UK). First, elute the impurities with 50 mM KPi buffer (pH = 7.2) containing 30 mM imidazole, and then elute the target protein with 50 mM KPi buffer (pH = 7.2) containing 200 mM imidazole. The purified protein fraction was concentrated by centrifugation at 4000*g* for 1 hour using Amicon ultrafiltration centrifuge tubes with a molecular weight cutoff of 10 kDa. The sample was then washed twice with 50 mM KPi buffer (pH = 7.2) to completely remove any residual imidazole. The purified proteins (10 μL) were loaded into 12% SDS PAGE to check the quality of purification (Fig. S1).

Expression and purification of AlkB

A 1% preculture of *E. coli* C43 (DE3) harbored pET-20b-*alkb* plasmid was grown overnight in LB medium containing 100 mg L^{-1} ampicillin at 30 °C with vigorous shaking (200 rpm). 5 L LB medium with 100 mg L^{-1} ampicillin was inoculated with the 2% (v/v) preculture and incubated at 30 °C until the optical density at OD_{600} reached 0.5, followed by the addition of 0.5 mM IPTG (final concentration) and 60 mg L^{-1} $FeCl_2{\cdot}4H_2O$ (final concentration). Then, the culture was incubated at 30 °C for 6 hours and harvested by centrifugation at 6000*g* for 10 minutes. Cell pellets were resuspended in buffer solution: 50 mM KPi buffer (pH = 7.2), 150 mM NaCl, 15% glycerol, 4 mM β-mercaptoethanol, followed by sonification. Disrupted cells were centrifuged at 12 000 rpm for 1 hour to remove insoluble cell debris. The supernatant was loaded onto the column packed with HisPrep™ FF 16/10 (Cytiva, Amersham, UK) and eluted with 50 mM KPi buffer (pH = 7.2) containing 200 mM imidazole, 150 mM NaCl, 15% glycerol, and 4 mM β-mercaptoethanol. The purified protein fractions were concentrated at 5000*g* for 1 hour using a 30 kDa Amicon centrifugal filter. The blocked protein (10 μL) was loaded onto a 12% SDS-PAGE molecule for transient analysis to determine the blocking quality (Fig. S1). The sample was then flash-frozen in liquid nitrogen and stored at −80 °C for subsequent experiments.[30]

Expression and purification of CYP153A$_{Maq}$

CYP153A$_{Maq}$ was expressed and purified as previous report with some modifications.[33] *E. coli* BL21 (DE3) containing pET-20b-CYP153A$_{Maq}$ plasmid was inoculated into 6 mL TB medium containing 100 mg L^{-1} ampicillin and cultured overnight at 37 °C and 220 rpm to prepare seed culture. The preculture was transferred to 3 L TB medium at an inoculum of 1% (v/v) and ampicillin was added to a final concentration of 100 mg L^{-1}, and vitamin B1 to a final concentration of 1 mM to initiate the expansion culture. When the OD_{600} reaches approximately 0.6–0.8, add 0.2 mM IPTG (final concentration), 0.5 mM ammonium ferric citrate (final concentration), and 1 mM δ-aminolevulinic acid (final concentration). After culturing the culture at 20 °C for 18 hours, the cells were harvested by centrifugation at 6000*g* for 10 minutes at 4 °C. The cell pellets were resuspended in 50 mM KPi buffer (pH = 7.2), followed by sonification. After centrifugation, the supernatant was loaded onto the column packed with HisPrep™ FF 16/10 (Cytiva, Amersham, UK) and eluted with 50 mM KPi buffer (pH = 7.2) containing 200 mM imidazole. The purified protein fractions were concentrated at 4000*g* for 1 hour using a 30 kDa Amicon centrifugal filter and washed twice with 50 mM KPi buffer (pH = 7.2) to remove imidazole. Protein samples were fractionated and flash frozen using liquid nitrogen to be stored at −80 °C until used in further steps. The purified proteins (10 μL) were loaded into 12% SDS-PAGE to check the quality of purification (Fig. S1).

Expression and purification of Pdx

Pdx was expressed and purified as previous report with some modifications. *E. coli* BL21(DE3) containing pET-20b-Pdx plasmid was inoculated into 6 mL TB medium containing 100 mg L^{-1} ampicillin and cultured overnight at 37 °C and 220 rpm to prepare seed culture. The preculture was transferred to 3 L TB medium at an inoculum of 1% (v/v) and ampicillin was added to a final concentration of 100 mg L^{-1} to initiate the expansion culture. When the OD_{600} reaches approximately 0.6–0.8, add 0.2 mM IPTG (final concentration), 50 mg mL^{-1} $FeCl_2{\cdot}4H_2O$ (final concentration). The culture was incubated at 16 °C and 220 rpm for 18 hours. The cell pellet was then collected by centrifugation at 6000*g* for 10 minutes at 4 °C. The cell pellets were resuspended in 50 mM KPi buffer (pH = 7.2), followed by sonification. After centrifugation, the supernatant was loaded onto the column packed with HisPrep™ FF 16/10 (Cytiva, Amersham, UK) and eluted with 50 mM KPi buffer (pH = 7.2) containing 200 mM imidazole. The purified protein fractions were concentrated at 4000*g* for 1 hour using a 10 kDa Amicon centrifugal filter and washed twice with 50 mM KPi buffer (pH = 7.2) to remove imidazole. Protein samples were fractionated and flash frozen using liquid nitrogen to be stored at −80 °C until used in further steps. The purified proteins (10 μL) were loaded into 12% SDS-PAGE to check the quality of purification (Fig. S1).

Concentration assays

For most purified enzymes (including AlkB, EcALDH, $AcCO_6$, CatA, AlkG, PdR, Pdx), protein concentrations were determined using the Bradford assay. The specific enzyme concentrations were calculated by measuring the absorbance at 595 nm against a standard curve constructed with bovine serum albumin (BSA). The formula for calculating molar concentration is:

$$\text{Concentration } (\mu\text{M}) = \frac{\text{concentration (mg mL}^{-1})}{\text{molecular weight (kDa)}} \times 1000.$$

The active CYP153A$_{Maq}$ concentration was determined by CO titration.[27] In a fume hood, CO gas is slowly passed into the CYP153A$_{Maq}$ solution using a clean Pasteur pipette. The treated solution was then transferred to a cuvette and placed in a spectrophotometer from Molecular Devices (USA) for spectral scanning and data recording in the 300–500 nm wavelength range (Fig. S2).

$$\text{Concentration } (\mu\text{M}) = \frac{\Delta A_{450} - \Delta A_{490}}{0.091\ \text{mM}^{-1}\ \text{cm}^{-1}}.$$

Enzyme activity assays

The activity of AlkB was measured using a previously described spectrophotometric assay with some modifications.[49] The 200 μL reaction mixture contained 100 mM KPi buffer (pH = 8.0), 0.47 mg mL^{-1} AlkB, 0.60 mg mL^{-1} alkG and 2.80 mg mL^{-1} PDR (molar ratio of AlkB : AlkG : PdR = 1 : 3 : 6), 0.15 mM NADH and 2 mM dodecane (5% DMSO as cosolvent) as substrate. The rate of NADH consumption was monitored at 340 nm for 2 min using a Multiskan sky plate reader (Thermo Fisher Scientific, Finland) at room temperature. The millimolar extinction coefficient of NADH (ε_{340}) was 6.22 mM^{-1} cm^{-1}. The background activity was determined by the addition of 5% DMSO, which does not contain dodecane. All samples were quantified as triplicates. The activity was expressed as units (U) per mg protein, where 1 U was defined as 1 μmol of dodecane consumed (consuming 1 μmol NADH) per min. The specific activity of AlkB was determined to be 0.13 ± 0.02 U mg^{-1}.

The enzymatic activity of $AcCO_6$ was measured at room temperature in a 500 μL reaction mixture comprising 100 mM KPi buffer (pH 8.0), 0.61 mg mL^{-1} $AcCO_6$, and 2 mM 12-hydroxydodecanoic acid. Following a 10 min incubation, the reaction was quenched by acidification with 10% (v/v) hydrochloric acid. Subsequently, the mixture was extracted using 500 μL Methyl *tert*-Butyl Ether (MTBE) containing 0.5 mM *n*-eicosane as an internal standard. All assays were performed in triplicate. One unit (U) of enzyme activity was defined as the amount of enzyme required to consume 1 μmol of 12-hydroxydodecanoic acid per minute. The specific activity of $AcCO_6$ was determined to be 4.3 ± 0. 2 mU mg^{-1}.

The activity of CYP153A$_{Maq}$ was measured using a spectrophotometric assay. The 200 μL reaction mixture contained 100 mM KPi buffer (pH = 8.0), 0.54 mg mL^{-1} CYP153A$_{Maq}$, 0.47 mg mL^{-1} PdR and 1.26 mg mL^{-1} Pdx (molar ratio of CYP153A$_{Maq}$: PdR : Pdx = 1 : 1 : 10), 0.15 mM NADH and 2 mM dodecanoic acid (5% DMSO as cosolvent) as substrate. The rate of NADH consumption was monitored at 340 nm for

2 min using a Multiskan sky plate reader (Thermo Fisher Scientific, Finland) at room temperature. The millimolar extinction coefficient of NADH (ε_{340}) was 6.22 mM^{-1} cm^{-1}. The background activity was determined by the addition of 5% DMSO, which does not contain dodecanoic acid. All samples were quantified as triplicates. The activity was expressed as units (U) per mg protein, where 1 U was defined as 1 μmol of 12-hydroxydodecanoic acid generated (consuming 1 μmol NADH) per min. The specific activity of $CYP153A_{Maq}$ was determined to be 0.17 ± 0.06 U mg^{-1}.

The activity of EcALDH was measured using a continuous spectrophotometric assay at room temperature. Activity toward dodecanal: the 200 μL reaction mixture comprised 100 mM KPi buffer (pH 8.0), 0.54 mg mL^{-1} EcALDH, 0.15 mM NAD^+, and 2 mM dodecanal (using 5% DMSO as a cosolvent). The rate of NADH generation was monitored continuously at 340 nm for 2 min using a Multiskan Sky plate reader (Thermo Fisher Scientific, Finland). A millimolar extinction coefficient (ε_{340}) of 6.22 mM^{-1} cm^{-1} was used for NADH quantification. Background activity was corrected by utilizing a substrate-free control containing 5% DMSO. All assays were performed in triplicate. One unit (U) of activity was defined as the amount of enzyme required to generate 1 μmol of NADH per minute, corresponding to the oxidation of 1 μmol of dodecanal. The specific activity of EcALDH toward dodecanal was determined to be 0.36 ± 0.01 U mg^{-1}. Activity toward 12-oxododecanoic acid: due to the commercial unavailability of a 12-oxododecanoic acid standard, the substrate was prepared enzymatically using $AcCO_6$. Briefly, a 500 μL reaction mixture containing 100 mM KPi buffer (pH 8.0), 100 μM $AcCO_6$, 10 μM CatA, and 2 mM 12-hydroxydodecanoic acid (with 5% DMSO as a cosolvent) was incubated for 8 h under magnetic stirring at 500 rpm. Following the reaction, proteins were removed *via* ultrafiltration using an Amicon Ultra centrifugal filter (10 kDa MWCO) to harvest the generated 12-oxododecanoic acid. Subsequently, the EcALDH activity assay was performed in a final volume of 200 μL containing 100 mM KPi buffer (pH 8.0), 0.54 mg mL^{-1} EcALDH, 0.15 mM NAD^+, and the obtained filtrate as the substrate. NADH generation was monitored at 340 nm for 2 min, as described above. One unit (U) of activity was defined as the generation of 1 μmol of NADH per minute, corresponding to the formation of 1 μmol of dodecanedioic acid. The specific activity of EcALDH toward 12-oxododecanoic acid was determined to be 0.32 ± 0.01 U mg^{-1}.

Multi-enzymatic conversion from dodecane to dodecanoic acid

The conversion of dodecane to dodecanoic acid was performed using a 7 mL sealed vial at room temperature. The 500 μL reaction mixture contained 100 mM KPi buffer (pH = 8.0), 25 μM (0.15 U mL^{-1}) AlkB, 75 μM AlkG, 150 μM PdR (molar ratio of AlkB : AlkG : PdR = 1 : 3 : 6), 15 μM (0.29 U mL^{-1}) EcALDH, 25 μM NADH, and 0.75% (v/v) dodecane as substrate. To ensure the uniform dispersion of the highly hydrophobic dodecane in the aqueous system, the mixture was briefly sonicated at 40 kHz for 40 s prior to the reaction. The reactions were started by the injection of 3 mL of air and were incubated under continuous magnetic stirring at 500 rpm. The generated products were extracted using MTBE, with 0.5 mM eicosane as an internal standard. The reaction pathway was shown as Scheme S2.

The conversion from dodecanoic acid to dodecanedioic acid

The one-pot conversion of dodecane to dodecanedioic acid was achieved through two consecutive functional modules. Module I is a two-step C–H bond oxygen functionalization reaction of dodecane. The module I reaction was performed using the method mentioned in the above section of "Multi-enzymatic concersion from dodecane to dodecanoic acid". After 6 hours of the Module I reaction, the reaction mixture was used directly without any intermediate enzyme removal steps. This one-pot strategy ensures that the endogenous NADH pool regenerated during Module I remains completely intact within the mixture, naturally carrying over to drive the subsequent catalytic cycles. Module II generates dodecanedioic acid by continuously oxidizing the C–H bond at the ω position of the dodecanoic acid. The reaction of Module II was initiated sequentially by adding 30 mM $MgCl_2$, 20 μM (0.19 U mL^{-1}) $CYP153A_{Maq}$, 20 μM PdR, 200 μM Pdx (molar ratio of $CYP153A_{Maq}$: PdR : Pdx = 1 : 1 : 10), 100 μM (0.03 U mL^{-1}) $AcCO_6$, 30 μM (0.52 U mL^{-1}) EcALDH, and 10 μM CatA directly into the same reaction vessel.

GC analysis

Gas chromatography was used to detect and quantify the intermediates and products of the reaction. Samples containing dodecanol, dodecanal, dodecanoic acid, 12-hydroxydodecanoic acid, and 12-oxododecanoic acid were analyzed directly following acidification with 10% HCl and extraction with MTBE, which contained 0.5 mM eicosane as an internal standard. Experiments were conducted using a FULI INSTRUMENTS GC9790 plus (Zhejiang, China) equipped with an Agilent HP-5 column (30 m × 0.32 mm × 0.25 μm). The inlet temperature was held at 240 °C with a 1.0 mL min^{-1} column flow rate and nitrogen as the carrier gas. 2 μL samples were injected onto the column. The oven temperature was held at 60 °C for 1 min, then ramped to 200 °C at 20 °C min^{-1} and held at 200 °C for 15 min. Given its significantly higher polarity and lower volatility compared to the monoacid, dodecanedioic acid cannot be accurately detected directly under these conditions. Therefore, as described in Fig. S6a of the SI, all samples for its quantification were subjected to derivatization prior to GC analysis.

Results and discussion

Design of the multi-enzymatic deep conversion system of dodecane

Herein, the multi-enzymatic deep conversion of dodecane was employed as a model reaction. As illustrated in Fig. 1, the transformation of dodecane to dodecanedioic acid proceeds through two consecutive and functionally integrated modules.

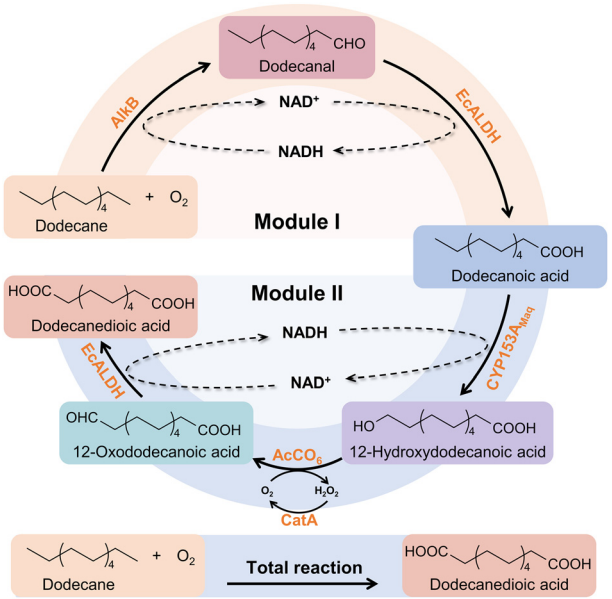

Fig. 1 The schematic representation of the multi-enzyme alkane deep conversion system that converts dodecane to dodecanedioic acid. AlkB: alkane hydroxylase, EcALDH: aldehyde dehydrogenase, $CYP153A_{Maq}$: P450 monooxygenase, $AcCO_6$: engineered choline oxidase, CatA: catalase.

Module I involves a two-step, regioselective terminal C–H oxyfunctionalization of dodecane enabled by internal cofactor recycling. Specifically, dodecane is first oxidized to dodecanal *via* AlkB-catalyzed regioselective terminal C–H hydroxylation, consuming NADH. Subsequently, dodecanal is further oxidized to dodecanoic acid by EcALDH. Notably, during this process, the NAD^+ generated in the AlkB-catalyzed hydroxylation step is simultaneously reduced back to NADH by EcALDH, thereby establishing a closed hydrogen-borrowing cycle. This internally balanced cofactor regeneration eliminates the need for external reducing agents and underpins the sustainability and atom economy of the overall transformation.

Module II enables the oxidation of the ω-C–H bond of dodecanoic acid to afford dodecanedioic acid *via* a designed enzymatic cascade that features internal cofactor recycling. In this module, the dodecanoic acid produced in Module I undergoes regioselective ω-hydroxylation catalyzed by $CYP153A_{Maq}$, consuming NADH and generating NAD^+ to form 12-hydroxydodecanoic acid. $AcCO_6$ subsequently oxidizes the hydroxyl intermediate to yield 12-oxododecanoic acid, with molecular oxygen serving as the terminal oxidant and H_2O_2 formed as a byproduct. To prevent oxidative deactivation of the enzymatic system, catalase (CatA) rapidly decomposes H_2O_2 *in situ*. Finally, EcALDH utilizes the NAD^+ generated in the $CYP153A_{Maq}$-catalyzed step to oxidize the aldehyde group to a carboxyl group, producing dodecanedioic acid and regenerating NADH. This sequence closes a second hydrogen-borrowing cycle within Module II.

Overall, driven by two integrated hydrogen-borrowing cycles, the chemically inert dodecane is converted to dodecanedioic acid using molecular oxygen as the sole terminal oxidant under ambient conditions. The tight coupling of regioselective C–H oxyfunctionalization with internal cofactor regeneration eliminates the need for external reducing agents or sacrificial cofactors, thereby maximizing atom economy and process sustainability, which provides a green strategy for the deep oxidation of chemically inert alkanes.

Module I: optimization of dodecane loading

AlkB requires auxiliary redox partners, including AlkG and AlkT, to shuttle electrons from NADH to the diferric active site of AlkB, thereby enabling regioselective hydroxylation of the terminal C–H bond.[28,50,51] To overcome the low expression level of AlkT in *Escherichia coli*, we adopted a substitution strategy reported in previous studies, employing putidaredoxin reductase (PdR, UniProt: P16640) from *Pseudomonas putida* as a functional surrogate for AlkT (Scheme S1).[28,30]

To identify the optimal reaction conditions for Module I, we systematically evaluated the effect of *n*-dodecane loading on product distribution. As shown in Fig. 2a and Fig. S3, the cumulative concentrations of dodecanal and dodecanol increased with increasing *n*-dodecane loading. An optimal *n*-dodecane concentration of 0.75% (v/v) was identified, affording the highest accumulation of dodecanal (0.13 mM) along with only a minor amount of dodecanol (0.01 mM) after 2 h of reaction at an AlkB concentration of 10 μM.

Although increasing substrate loading can enhance overall conversion efficiency, further increases in *n*-dodecane concentration to 1–2% (v/v) resulted in a pronounced decrease in dodecanal accumulation (Fig. 2a). At these higher loadings, excess *n*-dodecane induces the formation of an aqueous–organic biphasic system. Maintaining such a system requires vigorous stirring to increase the interfacial area and facilitate mass transfer, which promotes enzyme adsorption at the phase boundary. This interfacial adsorption disrupts the electrostatic, hydrophobic, and hydrogen-bonding interactions that stabilize protein structure, ultimately leading to irreversible enzyme denaturation.[52]

Module I: the conversion from dodecane to dodecanoic acid

The optimal concentration of the alkane hydroxylase AlkB was first evaluated. As shown in Fig. 2b, increasing the AlkB concentration initially led to enhanced dodecanal formation, followed by a decline at higher enzyme loadings. Dodecanal production reached a maximum of 0.56 mM at an AlkB concentration of 25 μM (0.15 U mL^{-1}). However, further increasing the enzyme concentration to 30 and 35 μM resulted in a pronounced decrease in product accumulation. This decline can be attributed to intermolecular interactions at high enzyme concentrations. Beyond a critical threshold, AlkB molecules aggregate to form higher-order assemblies, thereby reducing the effective catalytic surface area and inducing conformational changes that compromise enzymatic activity.[53,54] Consequently, an AlkB concentration of 25 μM (0.15 U mL^{-1}) was identified as optimal, providing sufficient catalytic activity

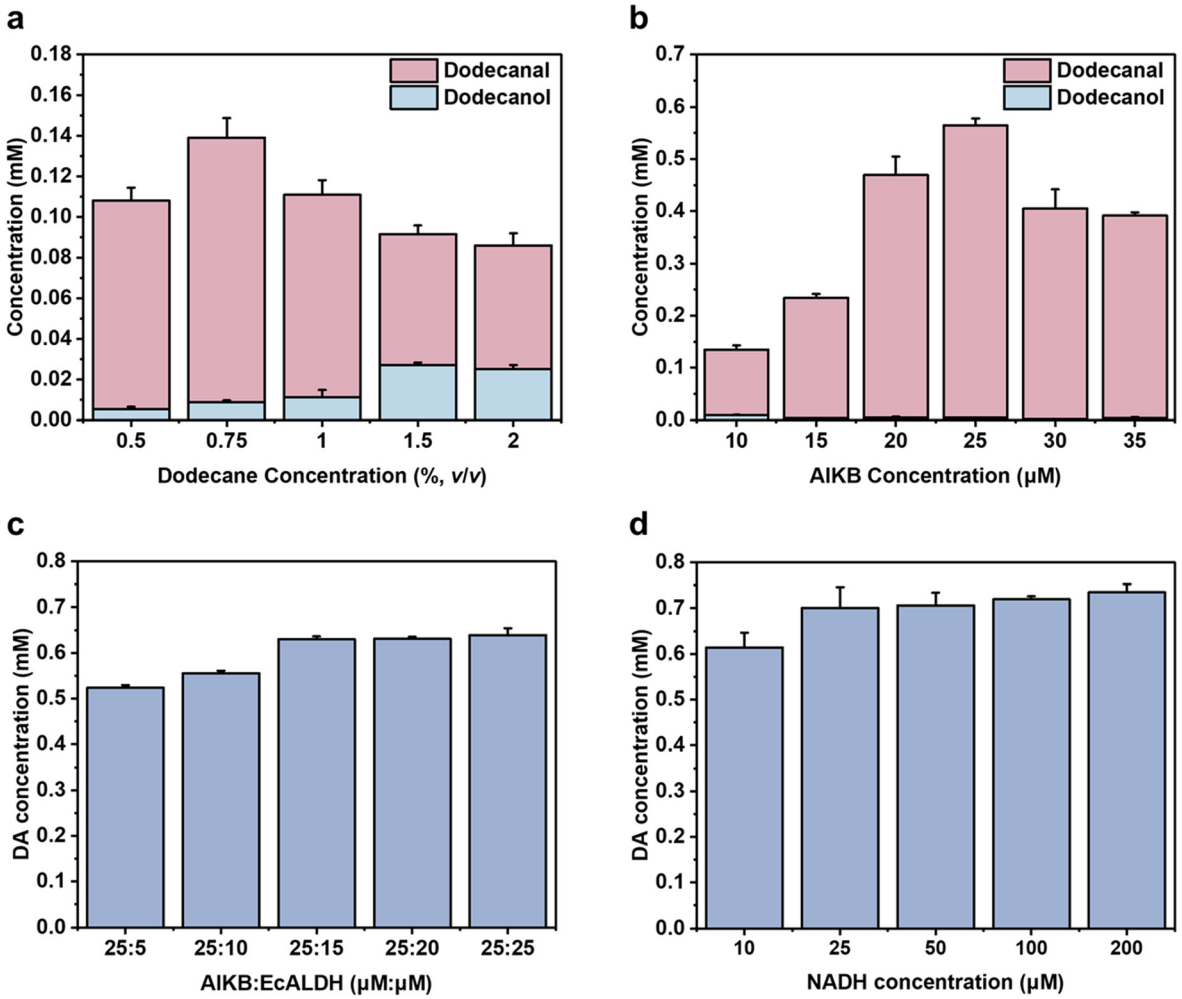

Fig. 2 Optimization of the reaction system in Module I. (a) Optimization of dodecane loading, the AlkB concentration was fixed at 10 μM (0.06 U mL^{-1}). The reactions were performed in a 7 mL sealed vial with magnetic string at room temperature. The 500 μL reaction mixture contained 100 mM KPi buffer (pH = 8.0), 10 μM (0.06 U mL^{-1}) AlkB, 30 μM AlkG, 60 μM PdR (molar ratio of AlkB : AlkG : PdR = 1 : 3 : 6), 4 mM NADH and dodecane at different concentrations of 0.5–2% (v/v) as substrate. The reactions were performed at room temperature for 2 h. (b) The optimization of AlkB concentration under a fixed dodecane loading of 0.75% (v/v). The reaction conditions were the same as in a. (c) The optimization of AlkB : EcALDH ratio with the AlkB concentration fixed at 25 μM (0.15 U mL^{-1}). The reactions were performed at room temperature for 2 h. (d) The optimization of NADH concentration with the molar ratio of AlkB to EcALDH fixed at 25 : 15 (μM : μM). The reactions were performed at room temperature for 2 h. All data is presented as the mean value of three independent technical experiments (n = 3), and the error bars indicate ± SD.

while avoiding the detrimental effects associated with enzyme aggregation.

In the biocatalytic conversion of dodecane to dodecanedioic acid, the central transformation involves the stepwise oxidation of the α,ω-terminal methyl C–H bonds to carboxyl groups. Within this cascade, dodecanoic acid serves as a key intermediate, as it constitutes the essential precursor for subsequent dual-terminal functionalization. As illustrated in Fig. 1, this transformation is achieved through the synergistic action of AlkB and EcALDH. AlkB first catalyzes the regioselective over-oxidation of the terminal C–H bond of dodecane to form dodecanal, which is subsequently oxidized by EcALDH to yield dodecanoic acid (Fig. S4). This sequence establishes the chemical foundation for the downstream ω-oxidation step that leads to the formation of dodecanedioic acid. Notably, the AlkB- and EcALDH-catalyzed reactions are intrinsically coupled through a hydrogen-borrowing mechanism, in which the NADH consumed during AlkB-mediated hydroxylation is regenerated by EcALDH during aldehyde oxidation, thereby forming a closed and self-sustaining redox cycle (Scheme S2).

The molar ratio of AlkB to EcALDH in Module I was optimized to ensure coordinated reaction rates between the two enzymes. As shown in Fig. 2c, the optimal AlkB : EcALDH ratio was determined to be 25 : 15 (μM : μM), under which 0.63 mM dodecanoic acid was produced within 2 h in the presence of 4 mM NADH. Notably, no accumulation of the intermediates, dodecanal or dodecanol, was observed, indicating efficient coupling of the two catalytic steps. Considering the high cost of NADH, its dosage was further optimized. As illustrated in Fig. 2d, increasing the NADH concentration from 10 to 25 μM

led to a marked improvement in reaction efficiency and dodecanoic acid accumulation. At an NADH concentration of 25 μM, the dodecanoic acid concentration reached 0.70 mM after 2 h, again without detectable accumulation of intermediates. Further increases in NADH concentration did not result in additional product formation, indicating that the reaction was no longer limited by cofactor availability. Significantly, the implementation of the hydrogen-borrowing strategy for *in situ* NADH regeneration substantially enhanced the efficiency of AlkB-catalyzed terminal C–H hydroxylation. As shown in Fig. 2d, the regeneration system yielded 0.70 mM dodecanoic acid after 2 h, corresponding to effective activation of 0.70 mM dodecane. In contrast, direct supplementation with 4 mM NADH resulted in the formation of only 0.56 mM dodecanal and 0.01 mM dodecanol (Fig. 2b), corresponding to merely 0.57 mM activated dodecane.

This comparison demonstrates that hydrogen-borrowing-mediated NADH regeneration not only significantly reduces cofactor consumption but also improves the overall efficiency of alkane conversion. Under the optimized conditions with 25 μM NADH, the cumulative concentration of dodecanoic acid continued to increase over time, reaching a maximum of 1.53 mM after 6 h (Fig. 3). Dodecanal was detected only during the first 2 h of the reaction, whereas dodecanol was not detected throughout the process. These results indicate that the hydrogen-borrowing cycle enables highly efficient and sustained NADH regeneration, thereby continuously driving the conversion of dodecane to dodecanoic acid.

It should be noted that while the canonical two-step monooxygenation by AlkB theoretically consumes two equivalents of NADH against the regeneration of one NADH by EcALDH, our system experimentally achieved a >60-fold turnover of the initial NADH pool. In accordance with established phenomena in *in vitro* multienzyme cascades, this outstanding stoichiometric sufficiency is likely facilitated by the trace retention of the *E. coli* endogenous enzymatic network within the partially purified system.[39,55–59] These background oxidoreductases may either assist in the NAD^+-dependent dehydrogenation of the intermediate alcohol or drive a slow, continuous background NADH regeneration by utilizing residual buffer components (*e.g.*, glycerol) as sacrificial electron donors. This synergistic microenvironment effectively compensates for the theoretical stoichiometric deficit, maintaining the thermodynamic viability of the internal hydrogen-borrowing loop.

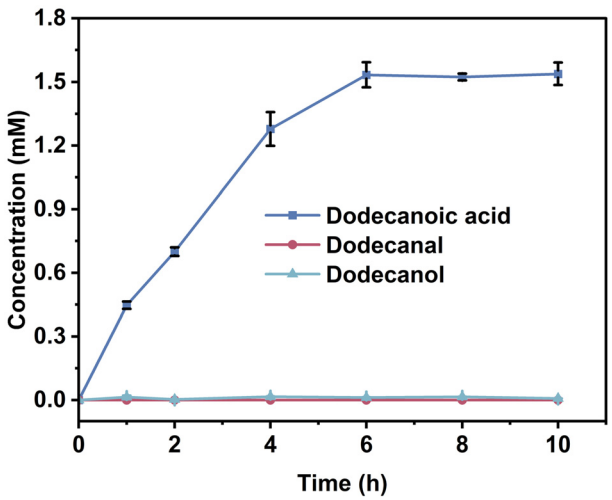

Fig. 3 The tracking of concentrations of dodecanol, dodecanal, and dodecanoic acid follows a time course. The reactions were performed in a 7 mL sealed vial with magnetic string at room temperature. The 500 μL reaction mixture contained 100 mM KPi buffer (pH = 8.0), 25 μM (0.15 U mL^{-1}) AlkB, 75 μM AlkG, 150 μM PdR (molar ratio of AlkB : AlkG : PdR = 1 : 3 : 6), 15 μM (0.29 U mL^{-1}) EcALDH, 25 μM NADH and 0.75% (v/v) dodecane as substrate. All data is presented as the mean value of three independent technical experiments (n = 3), and the error bars indicate ± SD.

Module II: the conversion from dodecanoic acid to dodecanedioic acid

In Module I, the terminal C–H bond of dodecane is oxyfunctionalized to form a carboxyl group. Building on this initial oxygen functionalization, we next introduced a carboxyl group at the ω-position to achieve complete conversion of dodecane to dodecanedioic acid. As illustrated in Fig. 1, dodecanoic acid (DA) is sequentially transformed into 12-hydroxydodecanoic acid (12-HDA) and 12-oxododecanoic acid (12-ODA) through the cascade catalysis of $CYP153A_{Maq}$ and $AcCO_6$, respectively, and is finally oxidized to dodecanedioic acid (DDA) by EcALDH (Fig. S5 and S6a, b). $CYP153A_{Maq}$ catalyzes the regioselective ω-hydroxylation step, thereby initiating the second terminal functionalization required for the formation of α,ω-dicarboxylic acids.[35] To support the catalytic activity of $CYP153A_{Maq}$, an electron transfer chain comprising putidaredoxin reductase (PdR) and putidaredoxin (Pdx) from *Pseudomonas putida* was employed, with NADH serving as the electron donor (Scheme S3).[60] Notably, $CYP153A_{Maq}$ and EcALDH operate synergistically to establish a second integrated hydrogen-borrowing cycle, in which the NADH consumed during $CYP153A_{Maq}$-catalyzed ω-hydroxylation is efficiently regenerated by EcALDH during the subsequent aldehyde oxidation step (Scheme S4). $AcCO_6$ catalyzes the oxidation of 12-hydroxydodecanoic acid to 12-oxododecanoic acid using molecular oxygen as the oxidant, concomitantly generating H_2O_2 as a byproduct.[46] In this cascade system, $AcCO_6$ bridges the two hydrogen-borrowing catalytic half-cycles of $CYP153A_{Maq}$ and EcALDH, thereby enabling synergistic operation of the entire reaction pathway.

In Module II, $CYP153A_{Maq}$ utilizes heterologous redox partners, PdR and Pdx, to drive the ω-hydroxylation of dodecanoic acid. The lack of native evolutionary co-adaptation between $CYP153A_{Maq}$ and these redox partners may lead to suboptimal protein–protein interactions, thereby limiting electron transfer efficiency. Divalent cations, particularly Mg^{2+}, play a crucial role in reconstituted P450 systems. Research indicates that Mg^{2+} facilitates the functional coupling between the redox partner and the P450 heme domain. This stabilized interaction stimulates electron flow, specifically accelerating the rate-limit-

ing reduction of the ferric P450-substrate complex (Fe^{3+}–Fe^{2+}), thereby driving a significant enhancement in overall oxidation turnover.[61] To address this limitation, the Mg^{2+} concentration in Module II was systematically optimized (Fig. 4a). 12-Hydroxydodecanoic acid (12-HDA) was detected across all tested Mg^{2+} concentrations, and its yield increased markedly as Mg^{2+} concentration increased from 10 to 30 mM, reaching a maximum at 30 mM (Fig. 4a). However, a further increase to 40 mM Mg^{2+} resulted in a decline in product formation. This decrease is likely attributable to excessive ionic strength. Physiologically, electron transfer complexes rely on electrostatic steering forces to guide the redox partner to the P450 proximal face. However, supra-optimal Mg^{2+} concentrations induce strong charge shielding which masks the surface charge complementarity and disrupts the critical interfacial salt bridges required for the effective docking between redox partners and $CYP153A_{Maq}$, thereby hindering the rate-limiting electron transfer step.[61,62] To further enhance the overall conversion efficiency, the enzyme ratios in Module II were optimized better to synchronize the reaction rates of the individual catalytic steps. By systematically varying the concentrations of $CYP153A_{Maq}$, $AcCO_6$, and EcALDH, an optimal molar ratio of 20 : 100 : 30 (μM : μM : μM) was identified (Fig. 4b and Fig. S7a, b), enabling more efficient cascade operation.

As shown in Fig. 5, after 6 h of reaction in Module I, the Module II system was introduced to initiate DDA synthesis. Upon initiation, the concentration of 12-HDA increased rapidly, reaching a maximum of 0.39 mM within 1 h, and was subsequently consumed efficiently, decreasing to only 0.003 mM after 6 h. In parallel, the concentration of DDA increased continuously throughout the reaction, reaching a maximum of 1.49 mM after 6 h. Notably, no accumulation of 12-ODA was observed throughout the conversion process, indicating rapid and efficient turnover of this intermediate within the cascade. Based on these results, the conversion efficiency of dodecanoic acid generated in Module I to DDA *via* Module II was calculated to be 97.4%. These findings clearly demonstrate that the hydrogen-borrowing cycle effectively drives the $CYP153A_{Maq}$-catalyzed ω-hydroxylation and subsequent oxidation steps, enabling highly efficient and tightly coupled conversion within the cascade system. Overall, we established a multi-enzyme cascade system driven by dual internal hydrogen-borrowing cycles for the deep oxidation of dodecane to dodecanedioic acid, which demonstrates significant green manufacturing potential as highlighted by a comparison with industrial chemical oxidation (butadiene route) and microbial fermentation (Table S1). Unlike chemical methods that rely on precious metals and harsh conditions, our approach achieves exclusive terminal C–H bond activation under mild conditions, preventing short-chain byproduct formation. Furthermore, compared to fermentation which consumes glucose for cofactor regeneration, our system utilizes internal hydrogen-borrowing for cofactor self-sufficiency. This design significantly enhances atom economy, presenting a sustainable, environmentally friendly route for long-chain dicarboxylic acid production.

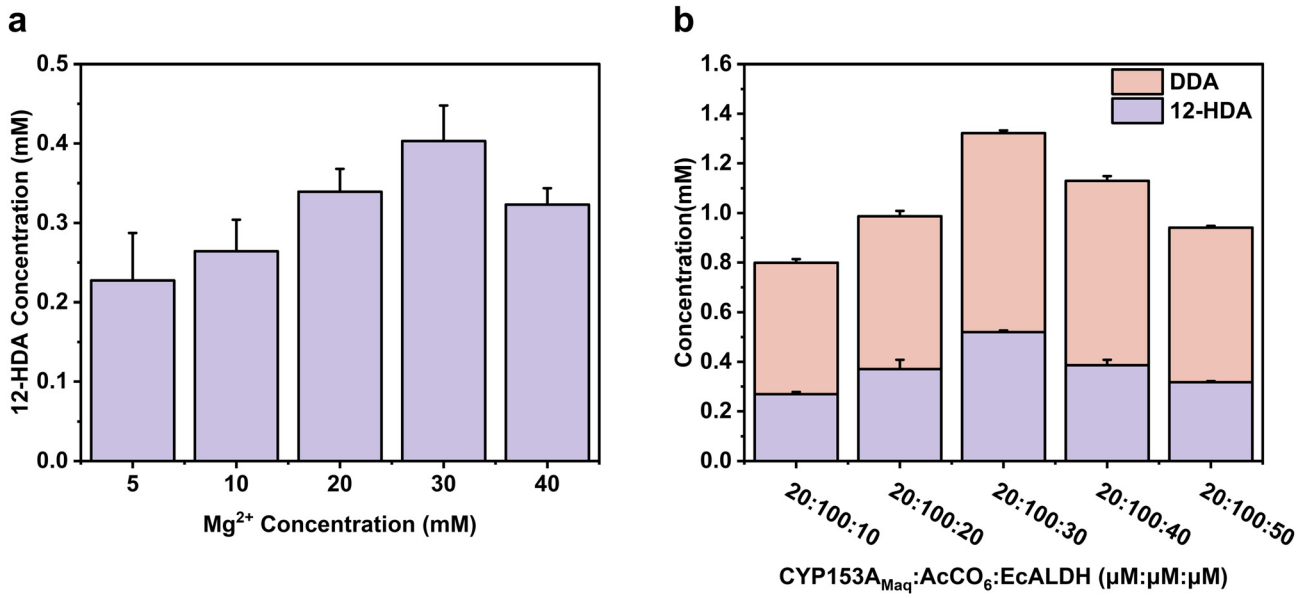

Fig. 4 Optimization of the reaction system in Module II. (a) Optimization of the Mg^{2+} concentration. With the $CYP153A_{Maq}$ concentration fixed at 10 μM (0.10 U mL^{-1}). The reactions were performed in a 7 mL sealed vial with magnetic string at room temperature. The 500 μL reaction mixture contained 100 mM KPi buffer (pH = 8.0), 10 μM (0.10 U mL^{-1}) $CYP153A_{Maq}$, 10 μM PdR, 100 μM Pdx (molar ratio of $CYP153A_{Maq}$: PdR : Pdx = 1 : 1 : 10), 4 mM NADH, 2 mM dodecanoic acid and Mg^{2+} at different concentrations (5–40 mM) as substrate. The reactions were performed at room temperature for 1 h. (b) Optimization of the enzyme ratio for $CYP153A_{Maq}$: $AcCO_6$: EcALDH. With a fixed concentration of $CYP153A_{Maq}$ at 20 μM (0.19 U mL^{-1}) and $AcCO_6$ at 100 μM (0.03 U mL^{-1}), EcALDH was added in varying proportions. All data is presented as the mean value of three independent technical experiments (n = 3), and the error bars indicate ± SD.

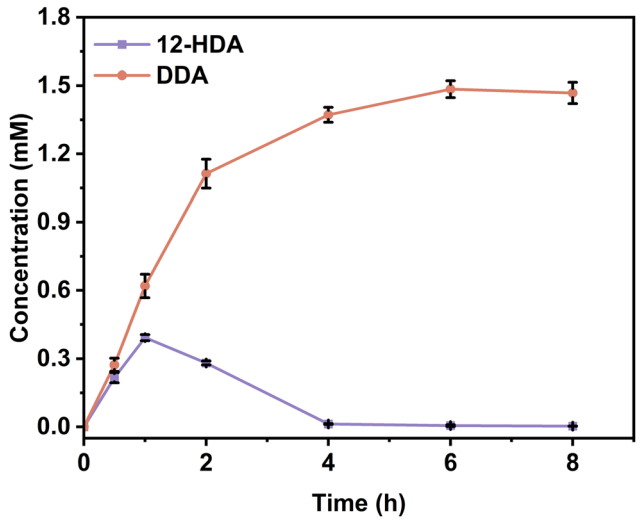

Fig. 5 The tracking of concentrations of 12-hydroxydodecanoic acid (12-HDA), 12-oxododecanoic acid (12-ODA) and dodecanedioic acid (DDA) following a time course. The reactions were performed in a 7 mL sealed vial with magnetic string at room temperature. The 500 μL reaction mixture contained 100 mM KPi buffer (pH = 8.0), 25 μM (0.15 U mL^{-1}) AlkB, 75 μM AlkG, 150 μM PdR (molar ratio of AlkB : AlkG : PdR = 1 : 3 : 6), 15 μM (0.29 U mL^{-1}) EcALDH, 25 μM NADH, and 0.75% (v/v) dodecane as substrate. After 6 hours of the Module I reaction, the reaction mixture was used directly without any intermediate enzyme removal steps. The reaction of Module II was started by adding 30 mM $MgCl_2$, 20 μM (0.19 U mL^{-1}) $CYP153A_{Maq}$, 20 μM PdR, 200 μM Pdx (molar ratio of $CYP153A_{Maq}$: PdR : Pdx = 1 : 1 : 10), 100 μM (0.03 U mL^{-1}) $AcCO_6$, 30 μM (0.52 U mL^{-1}) EcALDH, and 10 μM CatA directly into the same reaction vessel. All data is presented as the mean value of three independent technical experiments (n = 3), and the error bars indicate ± SD.

Multi-enzyme cascade conversions of different chemically inert alkanes to dicarboxylic acids

Inspired by the efficient conversion of dodecane to dodecanedioic acid using the multi-enzyme cascade, we extended this strategy to a range of linear aliphatic hydrocarbons (C_6–C_{14}) to evaluate its substrate scope for α,ω-dicarboxylic acid synthesis. As summarized in Table 1, except for tetradecane, eight substrates (C_6–C_{13}) were successfully converted into their corresponding fatty acid intermediates in Module I. The concentrations of the fatty acids obtained were as follows: hexanoic acid (0.16 ± 0.01 mM), heptanoic acid (0.42 ± 0.02 mM), octanoic acid (0.67 ± 0.04 mM), nonanoic acid (2.10 ± 0.02 mM), decanoic acid (0.79 ± 0.03 mM), undecanoic acid (2.08 ± 0.18 mM), dodecanoic acid (1.53 ± 0.06 mM), and tridecanoic acid (0.88 ± 0.03 mM). Among these intermediates, the C_9–C_{13} fatty acids were further transformed into the corresponding α,ω-dicarboxylic acids *via* Module II. Specifically, azelaic acid (0.64 ± 0.01 mM), decanedioic acid (0.63 ± 0.01 mM), undecanedioic acid (1.41 ± 0.02 mM), dodecanedioic acid (1.49 ± 0.04 mM), and tridecanedioic acid (0.83 ± 0.02 mM) were obtained. Although C_6–C_8 alkanes were successfully oxidized to their corresponding fatty acids in Module I, no formation of the corresponding α,ω-dicarboxylic acids was observed in Module II. This limitation reflects the intrinsic substrate specificity of $CYP153A_{Maq}$ toward medium- to long-chain substrates (C_9–C_{20}).[36] Future efforts will focus on rational engineering of $CYP153A_{Maq}$ to constrain the substrate-binding pocket, as well as on mining natural ω-hydroxylases with inherent activity toward short-chain fatty acids, to enable efficient dual-terminal oxidation across a broader substrate range.

As a proof-of-concept study, the results summarized in Table 1 clearly demonstrate the technical feasibility of the proposed multi-enzyme cascade system for converting chemically inert C_9–C_{13} n-alkanes into the corresponding α,ω-dicarboxylic acids. The successful biosynthesis of this series of high-value monomers highlights the broad applicability and industrial versatility of the cascade, establishing a promising biotechnological platform for the sustainable valorization of inert alkanes into key precursors for pharmaceuticals, polymers, and fine chemicals. Azelaic acid (C_9), a first-line topical pharmaceutical ingredient for the treatment of acne and rosacea, exhibits antibacterial, anti-inflammatory, and keratinocyte-regulating properties.[63,64] Decanedioic acid (C_{10}) serves as a key monomer for high-performance polymers such as Nylon 6,10 and Nylon 10,10, which are widely used in automotive components and electronic housings, and is also a base material for high-temperature lubricating greases in aerospace and precision machinery applications.[65] Undecanedioic acid (C_{11}) is a critical feedstock for engineering plastics, particularly Nylon 11, which is employed in high-reliability components such as fuel lines and pneumatic braking systems; it is also used in the fragrance industry for the synthesis of high-grade musk compounds. Dodecanedioic acid (C_{12}) is an important monomer for the production of high-performance engineering plastics (including Nylon 6,12 and Nylon 12,12), specialty polymers, plasticizers, fragrances, and pharmaceutical intermediates.[66] Tridecanedioic acid (C_{13}) plays a significant role in the high-end fragrance industry as a core precursor for musk-T and luxury perfume formulations.[67] And it is also used in the synthesis of specialty engineering plastics such as Nylon 13,13 and Nylon 6,13.[68]

Conclusions

In this work, we have established a multi-enzyme cascade conversion system driven by dual internal hydrogen-borrowing cycles for the deep oxidation of chemically inert alkanes to α,ω-dicarboxylic acids. By coupling regioselective C–H oxyfunctionalization with tightly balanced cofactor regeneration, this strategy utilizes molecular oxygen as the sole terminal oxidant under mild conditions. This design not only eliminates the need for external reducing agents or sacrificial cofactors but also maximizes atom economy, demonstrating a highly efficient route for transforming inert alkanes into value-added monomers. Beyond the synthesis of DCA, this study establishes general design principles for constructing C–H functionalization cascades that apply to the sustainable production of a broader range of high-value chemicals. By integrating enzyme-catalyzed C–H activation with rational cascade

Table 1 The conversion of various hydrocarbons to dicarboxylic acids[a]

Module I			Module II		
Substrate[b]	Product I	Concentration (mM)	Product II	Concentration (mM)	Product II/Product I (%)
Hexane(C_6)	Hexanoic acid	0.16 ± 0.01	Adipic acid	n.d.	
Heptane(C_7)	Heptanoic acid	0.42 ± 0.02	Heptanedioic acid	n.d.	
Octane(C_8)	Octanoic acid	0.67 ± 0.04	Octanedioic acid	n.d.	
Nonane(C_9)	Nonanoic acid	2.10 ± 0.02	Azelaic acid	0.64 ± 0.01	30.5%
Decane(C_{10})	Decanoic acid	0.79 ± 0.03	Decanedioic acid	0.63 ± 0.01	79.7%
Undecane(C_{11})	Undecanoic acid	2.08 ± 0.18	Undecanedioic acid	1.41 ± 0.02	67.8%
Dodecane(C_{12})	Dodecanoic acid	1.53 ± 0.06	Dodecanedioic acid	1.49 ± 0.04	97.4%
Tridecane(C_{13})	Tridecanoic acid	0.88 ± 0.03	Tridecanedioic acid	0.83 ± 0.02	94.3%
Tetradecane(C_{14})	Tetradecanoic acid	n.d. [c]	Tetradecanedioic acid	n.d.	

[a] All product concentrations are presented as mean ± standard deviation (n = 3). [b] The concentration of all substrates was 0.75% (v/v). [c] Not determined because of a very low conversion.

design inspired by synthetic biology, this work advances green manufacturing strategies that operate under mild conditions and avoid the energy- and emission-intensive steps characteristic of conventional petrochemical processes. Notably, the successful implementation of an internal hydrogen-borrowing cycle within a minimal four-enzyme, cell-free system demonstrates an effective strategy for biocatalytic process design, providing a practical blueprint for atom-economical and economically viable production of redox-intensive chemicals.

While the current space–time yield and final titer of this proof-of-concept *in vitro* cascade cannot yet compete with mature industrial fermentation or chemical processes, it establishes a foundational methodology. Future bioprocess engineering, such as enzyme immobilization and continuous-flow application, will be essential to optimize these quantitative parameters for industrial scale-up.

Author contributions

Zhijun Kong: writing – original draft, methodology, investigation, and data curation. Weihan Sun: investigation and discussion. Wenjin Dong: review & editing. Su Song: enzyme preparation. Li Ma: review & editing, and resources. Shengying Li: writing – review & editing, and resources. Hui Chen: writing – review & editing, supervision, resources, and funding acquisition. The manuscript was written through the contributions of all authors. All authors have approved the final version of the manuscript.

Conflicts of interest

There are no conflicts to declare.

Data availability

All experimental data supporting the findings of the article are available in the main text or supplementary information (SI). Supplementary information is available. See DOI: https://doi.org/10.1039/d6gc00241b.

Acknowledgements

We thank the support from the National Key Research and Development Program of China (Grant No. 2025YFA0921300), the Natural Science Foundation of China (Grants No. 32371534, 32571464, and 32025001), the Young Talent Development Program of SKLMT (No. M2025YA02), and the Fundamental Research Funds of Shandong University (Grant No. 2023QNTD001).

References

1 G. Li, D. Huang, X. Sui, S. Li, B. Huang, X. Zhang, H. Wu and Y. Deng, *React. Chem. Eng.*, 2020, **5**, 221–238.
2 H. Lee, Y. E. C. Sugiharto, H. Lee, W. Jeon, J. Ahn and H. Lee, *Appl. Microbiol. Biotechnol.*, 2019, **103**, 1545–1555.
3 S. Gu, F. Zhu, L. Zhang and J. Wen, *J. Agric. Food Chem.*, 2024, **72**, 5555–5573.
4 Sebacic Acid Market Size Share and Growth Analysis Report: Forecast Trends and Outlook (2026–2035), https://www.expertmarketresearch.com/reports/sebacic-acid-market (accessed January 2026).
5 A. Castellan, J. C. J. Bart and S. Cavallaro, *Catal. Today*, 1991, **9**, 237–254.
6 K. Sato, M. Aoki and R. Noyori, *Science*, 1998, **281**, 1646–1647.
7 W. Niu, K. M. Draths and J. W. Frost, *Biotechnol. Prog.*, 2002, **18**, 201–211.
8 J. F. C. Steele and S. Wallace, *Nat. Chem.*, 2024, **16**, 838.
9 A. Corona, M. J. Biddy, D. R. Vardon, M. Birkved, M. Z. Hauschild and G. T. Beckham, *Green Chem.*, 2018, **20**, 3857–3866.
10 C. Grant, D. Deszcz, Y.-C. Wei, R. J. Martínez-Torres, P. Morris, T. Folliard, R. Sreenivasan, J. Ward, P. Dalby, J. M. Woodley and F. Baganz, *Sci. Rep.*, 2014, **4**, 5844.

11 Y. M. v. Nuland, G. Eggink and R. A. Weusthuis, *Appl. Environ. Microbiol.*, 2016, **82**, 3801–3807.
12 L. Zhang, X. Xiu, Z. Wang, Y. Jiang, H. Fan, J. Su, S. Sui, S. Wang, R. Wang, J. Li, J. Wang, N. Li and J. Wang, *Mol. Biotechnol.*, 2021, **63**, 544–555.
13 F. Wang, H. Sun, D. Deng, Y. Wu, J. Zhao, Q. Li and A. Li, *Adv. Sci.*, 2025, **12**, e2411938.
14 P. Buathong, N. Boonvitthya, G. Truan and W. Chulalaksananukul, *Int. Biodeterior. Biodegrad.*, 2019, **139**, 70–77.
15 J.-H. Ju, B.-R. Oh, S.-Y. Heo, Y.-U. Lee, J.-h. Shon, C.-H. Kim, Y.-M. Kim, J.-W. Seo and W.-K. Hong, *Bioprocess Biosyst. Eng.*, 2020, **43**, 33–43.
16 M. S. Smit, M. M. Mokgoro, E. Setati and J.-M. Nicaud, *Biotechnol. Lett.*, 2005, **27**, 859–864.
17 J. Lee, I. Cornet, K. De Sitter and I. Noëlle Adrienne Van Bogaert, *Bioresour. Technol.*, 2025, **419**, 132006.
18 N. N. Pham, C.-W. Chang, Y.-H. Chang, Y. Tu, J.-Y. Chou, H.-Y. Wang and Y.-C. Hu, *Metab. Eng.*, 2023, **77**, 76–88.
19 Y. Wang, P. Hu, J. Yang, Y.-A. Zhu and D. Chen, *Chem. Soc. Rev.*, 2021, **50**, 4299–4358.
20 X. Tang, X. Jia and Z. Huang, *Chem. Sci.*, 2018, **9**, 288–299.
21 J. J. H. B. Sattler, J. Ruiz-Martinez, E. Santillan-Jimenez and B. M. Weckhuysen, *Chem. Rev.*, 2014, **114**, 10613–10653.
22 M. C. Bryan, P. J. Dunn, D. Entwistle, F. Gallou, S. G. Koenig, J. D. Hayler, M. R. Hickey, S. Hughes, M. E. Kopach, G. Moine, P. Richardson, F. Roschangar, A. Steven and F. J. Weiberth, *Green Chem.*, 2018, **20**, 5082–5103.
23 H. M. L. D. Morton, *J. Org. Chem.*, 2016, **81**, 343–350.
24 J. F. Hartwig and M. A. Larsen, *ACS Cent. Sci.*, 2016, **2**, 281–292.
25 J. Wencel-Delord and F. Glorius, *Nat. Chem.*, 2013, **5**, 369–375.
26 M. S. Chen and M. C. White, *Science*, 2007, **318**, 783–787.
27 S. Rej, A. Das and N. Chatani, *Coord. Chem. Rev.*, 2021, **431**, 213683.
28 M. Yuan, S. Abdellaoui, H. Chen, M. J. Kummer, C. A. Malapit, C. You and S. D. Minteer, *Angew. Chem., Int. Ed.*, 2020, **59**, 8969–8973.
29 A. Schmid, J. S. Dordick, B. Hauer, A. Kiener, M. Wubbolts and B. Witholt, *Nature*, 2001, **409**, 258–268.
30 A. Wang, Y. Wang, Y. You, Z. Huang, X. Zhang, S. Li and H. Chen, *Angew. Chem., Int. Ed.*, 2024, **63**, e202410260.
31 Y.-F. Tsai, W.-I. Luo, J.-L. Chang, C.-W. Chang, H.-C. Chuang, R. Ramu, G.-T. Wei, J.-M. Zen and S. S. F. Yu, *Sci. Rep.*, 2017, **7**, 8369.
32 H. Alonso and A. Roujeinikova, *Appl. Environ. Microbiol.*, 2012, **78**, 7946–7953.
33 Y. M. van Nuland, F. A. de Vogel, G. Eggink and R. A. Weusthuis, *Microb. Biotechnol.*, 2017, **10**, 594–603.
34 S. M. Hoffmann, H.-R. Danesh-Azari, C. Spandolf, M. J. Weissenborn, G. Grogan and B. Hauer, *ChemCatChem*, 2016, **8**, 3234–3239.
35 D. He, Y. Chen, J. Shen, H. Yu, J. D. Keasling and X. Luo, *Metab. Eng.*, 2025, **88**, 240–249.
36 S. Honda Malca, D. Scheps, L. Kühnel, E. Venegas-Venegas, A. Seifert, B. M. Nestl and B. Hauer, *Chem. Commun.*, 2012, **48**, 5115–5117.
37 U. Hanefeld, F. Hollmann and C. E. Paul, *Chem. Soc. Rev.*, 2022, **51**, 594–627.
38 N. Losada-Garcia, Z. Cabrera, P. Urrutia, C. Garcia-Sanz, A. Andreu and J. M. Palomo, *Recent Advances in Enzymatic and Chemoenzymatic Cascade Processes*, 2020, **10**, 1258.
39 J. M. Sperl and V. Sieber, *ACS Catal.*, 2018, **8**, 2385–2396.
40 L. Yang, X. Mu, Y. Nie and Y. Xu, *Metab. Eng.*, 2021, **64**, 122–133.
41 Y. H. Kim and Y. J. Yoo, *Enzyme Microb. Technol.*, 2009, **44**, 129–134.
42 H. Gröger, W. Hummel, C. Rollmann, F. Chamouleau, H. Hüsken, H. Werner, C. Wunderlich, K. Abokitse, K. Drauz and S. Buchholz, *Tetrahedron*, 2004, **60**, 633–640.
43 S. Rissom, J. Beliczey, G. Giffels, U. Kragl and C. Wandrey, *Tetrahedron: Asymmetry*, 1999, **10**, 923–928.
44 Z.-X. Liu, Y.-D. Gao and L.-C. Yang, *JACS Au*, 2024, **4**, 877–892.
45 J. H. Schrittwieser, S. Velikogne, M. Hall and W. Kroutil, *Chem. Rev.*, 2018, **118**, 270–348.
46 R. S. Heath, W. R. Birmingham, M. P. Thompson, A. Taglieber, L. Daviet and N. J. Turner, *ChemBioChem*, 2019, **20**, 276–281.
47 G. Gadda, N. L. N. Powell and P. Menon, *Arch. Biochem. Biophys.*, 2004, **430**, 264–273.
48 J.-E. Jo, S. Mohan Raj, C. Rathnasingh, E. Selvakumar, W.-C. Jung and S. Park, *Appl. Microbiol. Biotechnol.*, 2008, **81**, 51–60.
49 H. Chen, T. Tang, C. A. Malapit, Y. S. Lee, M. B. Prater, N. S. Weliwatte and S. D. Minteer, *J. Am. Chem. Soc.*, 2022, **144**, 4047–4056.
50 J. T. Groves, L. Feng and R. N. Austin, *Acc. Chem. Res.*, 2023, **56**, 3665–3675.
51 X. Guo, J. Zhang, L. Han, J. Lee, S. C. Williams, A. Forsberg, Y. Xu, R. N. Austin and L. Feng, *Nat. Commun.*, 2023, **14**, 2180.
52 N. Doukyu and H. Ogino, *Biochem. Eng. J.*, 2010, **48**, 270–282.
53 R. J. Ellis and A. P. Minton, *Nature*, 2003, **425**, 27–28.
54 R. J. Ellis, *Trends Biochem. Sci.*, 2001, **26**, 597–604.
55 A. Alissandratos, *Biophys. Rev.*, 2020, **12**, 175–182.
56 B. J. Rasor, B. Vögeli, G. M. Landwehr, J. W. Bogart, A. S. Karim and M. C. Jewett, *Curr. Opin. Biotechnol.*, 2021, **69**, 136–144.
57 J. U. Bowie, S. Sherkhanov, T. P. Korman, M. A. Valliere, P. H. Opgenorth and H. Liu, *Trends Biotechnol.*, 2020, **38**, 766–778.
58 V. M. Bolanos-Garcia and O. R. Davies, *Biochim. Biophys. Acta, Gen. Subj.*, 2006, **1760**, 1304–1313.
59 C. Robichon, J. Luo, T. B. Causey, J. S. Benner and J. C. Samuelson, *Appl. Environ. Microbiol.*, 2011, **77**, 4634–4646.
60 E. O. D. Johnson and L.-L. Wong, *Catal. Sci. Technol.*, 2016, **6**, 7549–7560.

61 H. Yamazaki, Y.-F. Ueng, T. Shimada and F. P. Guengerich, *Biochemistry*, 1995, **34**, 8380–8389.
62 R. W. Kelley, J. R. Reed and W. L. Backes, *Biochemistry*, 2005, **44**, 2632–2641.
63 X. Feng, J. Shang, Z. Gu, J. Gong, Y. Chen and Y. Liu, *Clin., Cosmet. Invest. Dermatol.*, 2024, **17**, 2359–2371.
64 C. Mariano-Rodriguez, P. Nava-Martinez and V. L. Diaz-Molina, *Cureus*, 2025, **17**, e94491.
65 W.-Y. Jeon, M.-J. Jang, G.-Y. Park, H.-J. Lee, S.-H. Seo, H.-S. Lee, C. Han, H. Kwon, H.-C. Lee, J.-H. Lee, Y.-T. Hwang, M.-O. Lee, J.-G. Lee, H.-W. Lee and J.-O. Ahn, *Green Chem.*, 2019, **21**, 6491–6501.
66 I. Funk, N. Rimmel, C. Schorsch, V. Sieber and J. Schmid, *J. Ind. Microbiol. Biotechnol.*, 2017, **44**, 1491–1502.
67 D. McGinty, C. S. Letizia and A. M. Api, *Food Chem. Toxicol.*, 2011, **49**, S174–S182.
68 S. Samanta, J. He, S. Selvakumar, J. Lattimer, C. Ulven, M. Sibi, J. Bahr and B. J. Chisholm, *Polymer*, 2013, **54**, 1141–1149.